Denoising, Outlier/Dropout Correction, and Sensor Selection in Range-Based Positioning

Shixiong Wang, *Graduate Student Member, IEEE*, Zhongming Wu, and Andrew Lim

Abstract— Range-based target localization combines the range measurements and appropriate algorithms [such as time of arrival (TOA)] to determine the real-time position of a moving target not only in a satellite-denied environment but also for high-precision applications in an open (i.e., satellite-available) environment. However, the measurements from sensors always suffer from uncertainties, such as noises, outliers, dropouts, and biases, which make measurements not reliable enough to directly utilize in positioning. This article is, therefore, concerned with two kinds of sensor correction problems: 1) attenuating the noises, removing the outliers, and completing the dropouts and 2) identifying the discredited sensors and forbidding them from use. Specifically, we model a range measurement time series from a ranging sensor as a nonstationary stochastic process and then use a local polynomial to regress the mean function in an online manner. The derivatives of the mean function are identified as the state variables in the state space, and the Kalman filter is used to estimate the states. We will show that: 1) the proposed method is simple yet effective in denoising the measurements and correcting the outliers/dropouts with very high accuracy and precision and 2) the defined and estimated states can clearly reflect the pattern of one type of nonspecific anomaly contained in the range time series, which enables the recognition of the dysfunctional sensors.

Index Terms— Fault diagnosis, filtering, sensor correction, target localization, time of arrival (TOA), time series, ultrawideband (UWB).

I. INTRODUCTION

A. Subject Matter

THE reliability of sensors significantly influences the performances of the related upper level applications since not all the measurements from sensors are exact enough

for direct use. Taking the ultrawideband (UWB) ranging for range-based positioning [1], [2] as an example, there are several types of uncertainties contained in the original range time series, which are indispensable to eliminate and/or calibrate, mainly including: 1) random (e.g., thermal) noises [3]–[5] that are generally white Gaussian with known or partially known statistics; 2) line-of-sight (LOS) and non-LOS (NLOS) ranging errors [3], [5]–[9] that act as unknown but numerically positive sensor biases/outliers; 3) channel errors other than NLOS [10]; 4) outliers in LOS environments due, e.g., to processing delay in signal processor (SPor) or to queuing delay of SPor interrupters; 5) dropouts that may be sparse or sometimes successively occur due, e.g., to occlusion; and 6) nonspecific errors existing as unknown biases. While uncertainty types 1)–3) are widely reported and studied in the past, types 4)–6) are new UWB sensor phenomena that the authors of this article observed in some uncertain positioning conditions. This article, therefore, mainly considers three kinds of issues in obtaining the reliable range measurements for range-based positioning under uncertainty types 1) and 4)–6). We also discuss the random (e.g., thermal, finite bandwidth, and nonideal equipment [3]) noise attenuating problem because, up to date, there is still few efficient online methods to denoise a noised model-free signal (i.e., a noised time series). Specifically, we are addressing the following three issues.

1) Filtering the random noise for a range time series.
2) Examining the range time series measurements and correcting the dropouts/outliers therein.
3) Excluding unreliable sensor(s) from the sensor bank. We separately consider this issue because, sometimes, some uncertainties in measurements are hard [or even impossible (see Fig. 2)] to correct.

Remark 1: Different from traditional NLOS/LOS errors in UWB ranging that introduces not only a nonzero mean (i.e., bias) but also a heavy tail (i.e., outliers) in the ranging error distribution, the outliers/dropouts studied in this article introduce ***no*** biases to the error distribution. When outliers/dropouts are excluded, the error distribution becomes roughly *zero-mean* Gaussian. That is, we are not handling the traditional NLOS/LOS error elimination problem. Instead, we assume that the traditional NLOS biases/outliers ***have already been mitigated*** by representative solutions, e.g., [3], [6], [7], [9], and [11], and the LOS biases ***have been addressed*** by the simple yet practical linear regression method [5], [9], i.e., $\hat{r} = a \cdot r + b$ where r is the measured range, a and b are regression coefficients, and $\hat{r}$ is the calibrated range. Since the distributions of the dropouts

and the SPor-related outliers are unknown, multiple-modal (see Fig. 14), and time-variant so that the statistics-based solution, e.g., [6], is not applicable, and the dropouts and the SPor-related outliers do not change the typical NLOS/LOS channel impulse responses (namely, power delay profiles) so that the pattern recognition methods, e.g., [7] and [9], are not applicable, the newly raised three issues in this article cannot be handled by the traditional NLOS/LOS error elimination methods. Thus, this article provides a complementary solution that executes after the traditional NLOS/LOS error elimination process. □

B. Literature Review

As an example, the ranging sensors that this article adopts are, but, in general, not limited to, UWB sensors. First, we review the drawbacks of the existing filtering techniques (for random noises) and provide a new idea to do signal filtering. Second, we investigate the existing outlier/dropout correction methods and state the necessity of our research. Third, we overview the existing sensor selection strategies and formulate one new type of sensor selection problem.

1) High-Accuracy Denoising: Measurements from sensors always suffer from noises. Typically, such noises are stationary, white, and Gaussian. We aim to denoise the measurements to provide more precise information. As an example, in [4], the moving average method is used in denoising the UWB ranging measurements. There are two categories of methods applied for denoising in the literature. The first one is model-based [12] where the signal model and sensor model (i.e., the dynamics of the information system that generates this signal and the dynamics of the sensor that captures the signal) are required. However, although the model-based methods are accurate and precise, for a general sensor, such methodology is limited to use because we cannot (sometimes, have no need to) obtain the signal model. The second category is model-free and identified as classical signal processing [13] or time series analysis [14], which is widely used in general measurement denoising. However, this kind of method is innately limited for high-accuracy denoising since such methods are likely to introduce the (severe) phase delay (i.e., time delay) issue because the phase response of a finite impulse response (FIR) or infinite impulse response (IIR) filter is usually significantly nonzero [13]. Therefore, we are expected to develop a new method that has high accuracy as model-based methods and that does not require the true signal model as model-free methods. The motivation is that, since we cannot obtain the true underlying signal dynamics, we can design an approximated model for this signal to bridge the performance gap between the model-based methods and the model-free methods, just like Zhai and Ye [15] do, where the Wiener process model is used for the product's lifetime degradation series.

2) Outlier/Dropout Correction: Except for the well-known noises, there exist other uncertainties, such as outliers and package dropouts in range measurements. Such outliers/dropouts may be sparse or sometimes may be very dense (see Fig. 1). Usually, if we define the ranging error
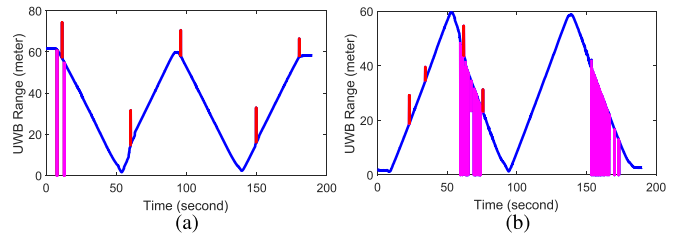

Fig. 1. Outliers/dropouts exist in UWB range measurements (real data from a field test). A dropout in range time series is due to the absence of a ranging-message package. When there is no reception of a message package at a time instant, we value the current range as zero. Therefore, in the figure, when the ranging measurement is zero-valued (magenta), it means that the current ranging message package is lost. The outliers are in red. (a) Outliers/dropouts are sparse. (b) Outliers/dropouts are extremely dense (e.g., at times around 60∼75 s).

as "measured range minus true range," dropouts introduce a heavy tail in the left-hand side of the error distribution, while outliers may introduce that in both the left- and right-hand sides. We are required to identify such outliers/dropouts and correct them afterward, i.e., using reasonable values to replace these wild values. The problem becomes harder for a scenario with very dense, or even successive, outliers/dropouts (e.g., see Fig. 1). The natural choice for outliers detection and removal is to use the M-estimation techniques [16], which is based on the measurement innovation (i.e., the difference between the predicted value and the true measured value). When the signal model is available and the predicted measurement is far away from the true measurement, two categories of methods can be adopted: 1) we treat the true measurement as an anomaly and directly use the prediction to replace (i.e., use a redescending influence function) [17]–[19], or we use a carefully selected value near the prediction to replace the true measurement (i.e., use a monotonic influence function) [20], [21] and 2) we use a robust filter gain to withstand the measurement uncertainties [22], [23]. When the signal model is unavailable, the outlier detection is only based on the collected measurement time series [24]–[26]. The nature of model-free methods is like the aforementioned predict-and-replace method in which a time series forecasting method is involved. The third choice for outlier rejection in range-based positioning is to jointly use all the range measurements (at a time instant) from all the available anchors and then design proper optimization strategies with proper criteria to identify and discard the outliers/dropouts from a subset of the anchors [27], [28]. However, for the outliers/dropouts correction problem formulated in this article, it is essentially a time series processing problem (namely, it is temporal, not spatial), which denies this methodology. Thus, the model-free methods that are only based on the time series measurements from one single sensor should be studied. In a nutshell, an efficient outliers'/dropouts' detection and correction strategy is to properly model the dynamics of the signal (like Zhai and Ye [15] do) and then use a proper predict-and-replace method (like Braei and Wagner [26] do). The predict-and-replace methods are preferable because we want to handle the very densely appeared, or successive, dropouts/outliers.
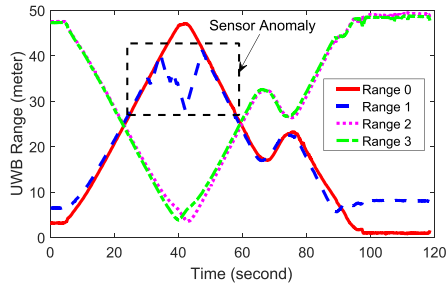
Fig. 2. Nonspecific (i.e., unknown of causing factors) sensor anomalies exist in the UWB range measurements (real data from a field test). We can see that Sensor 1 is problematic since its measurements in the rectangular are sharply changing against Sensor 0 (in fact, according to Section III-A, Sensor 0 and Sensor 1 should change in a roughly same way). Note that, for a macro-object, its moving speed is limited, meaning that the curve of the ranging measurements at a turning point should be smooth, with no sudden change. In this case, it is impossible for us to model this type of uncertainty/anomaly, so as to correct it afterward. Therefore, we can only identify it and exclude the corresponding sensor from functioning.

3) Fault Diagnosis and Sensor Selection: It is well-known that, in the 2-D positioning scenario, at least three anchors are required to generate the localization, while, in the 3-D case, at least four anchors are needed. However, in order to fuse information from redundant reference base stations, more than the least-required number of anchors are deployed and then use the pseudo-TDOA bootstrap strategy [29] or the least-squares methods [7], [30], [31] to improve the positioning accuracy. The bad news is that, when some of the sensors in this sensor bank are significantly unreliable, the participation of such sensors will, on the contrary, deteriorate the positioning performances [32]. This motivates us to identify those seriously diseased sensors and forbid them from functioning to maintain a desirable positioning accuracy. For example, Cong and Zhuang [6] suggested excluding the identified NLOS anchors and only use the LOS anchors for positioning. However, for some types of nonspecific uncertainties contained in range time series, we do not exactly know where it is from and how it evolves. As an instance, see the sensor anomalies in Fig. 2. Thus, we should design a method to quantitatively describe such errors and remove the unreliable Sensor 1 from the sensor bank. The main challenge is how to quantitatively describe this type of error and then construct the effective features to distinguish out its mother sensor. Note that whether a signal section of the whole signal is abnormal or not is application-specific, with no unified standards. For example, the "abnormal phenomena" discussed in [33, Fig. 1] are not considered as so in range measurements. On the other hand, the sensor selection also exists in Fig. 1 where the sensor that generates the dense outliers/dropouts [see Fig. 1(b)] should be excluded, because, under this circumstance, we may think that this sensor is extremely discredited so that we do not want to fetch information from it anymore instead of using some methods to rectify the diseased measurements. However, the most attention to sensor selection in the literature has been paid to the optimal and managerial functioning planning of sensors in consideration of energy-efficiency, tracking performances, and the like [34]–[36], namely, assuming that the sensors

have exactly known (and invariant) statistical information of measurement noises. This assumption may be harsh to satisfy in some real applications, as shown in Fig. 1. Although other focuses on sensor selection also take into account the negative influence of uncertainties in measurements, such as outliers [27], [32] or signal-obstructing (i.e., unable to receive a measurement signal) [37], the solution for the new type of observed uncertainty in Fig. 2 is lacking and expected. In summary, motivated by Gao *et al.* [38], we need to design a proper signal model for the range measurements that can not only differentiate the sharp-shaped anomalies but also describe the smooth- and quick-changing normal patterns. Note that the reason why we stress the property of quick-changing is that we aim to avoid the biases due to the dullness of the filtering method, as shown in Fig. 8(a). If the built signal model used for filtering is sluggish, biases will exist.

C. Contributions

As we can see, all the three issues require us to design a proper signal model for the ranging measurements, based on which the denoising, the outliers'/dropouts' detection and correction, and the description to one type of nonspecific anomalies in range measurements could be carried out. As a summary, the contributions are listed as follows:

1) modeling a range time series as a nonstationary stochastic process and identifying the derivatives of its mean function as state variables;
2) incorporating the derivatives of a time series into the filtering and forecasting processes to improve the filtering and forecasting accuracy, which is useful in outliers'/dropouts' detection and correction;
3) using the derivatives of the mean function of a range time series as the features to quantitatively describe a kind of nonspecific anomaly in measurements and then tell apart the morbid sensors from the sensor bank.

II. METHODOLOGY

A. Model a Signal and Define Its States

In Section I, we are motivated to construct a signal model for the range time series (i.e., range signal). It is obvious that the model has to encompass the following characteristics.

1) It is a stochastic process since it is noised.
2) It is nonstationary in the mean sense, i.e., the mean function is not a constant one.
3) It is a recursive-type time-series model because only in this way we can work on a sequential time series (namely, a signal that is a time function), not just block data.
4) It can exactly track the quick—but smooth—changing signal.
5) It can tell apart a sharp-changing subsequence of the range sequence as an anomaly.

Suppose that the range measurement (i.e., range time series) from a sensor is $x(t)$ or $x(n)$ with $t = nT$, where t is the continuous time, n is the discrete time, and T denotes the sampling time. We are inspired to use a deterministic function to model the mean function of $x(t)$ and a Gaussian white

stationary stochastic process to model the random part of $x(t)$. We have

$$x(t) = r(t) + s(t) \tag{1}$$

where $r(t) \geq 0$ (a range measurement is always nonnegative) is a deterministic function that models the true range and $s(t)$ is a white stationary Gaussian stochastic process that models the stationary Gaussian white (measurement) noises. The discrete version is

$$x(n) = r(n) + s(n) \tag{2}$$

where $E[s(n)s(n+k)] = 0$, $\forall k \neq 0$. When there are uncertainties other than noises in the range signal, the model will instead be

$$x(n) = r(n) + s(n) + b(n) + o(n) + d(n) \tag{3}$$

where $b(n)$ denotes the biases, $o(n)$ denotes the outliers, and $d(n)$ denotes the dropouts. As explained in Remark 1, we do not study the bias term in this article. Therefore, all efforts should be put on recovering the true range time series $r(n)$ from the uncertainty-corrupted range measurement time series $x(n)$. Since $r(t)$ is deterministic and continuous, we can find an order-sufficient polynomial $f(t)$ to uniformly approximate it. This is by the well-known Weierstrass approximation theorem. Generally, $f(t)$ is with the form of

$$f(t) = f_0 + f_1 t + f_2 t^2 + \cdots + f_k t^k + \cdots \tag{4}$$

where $f_0, f_1, f_2, \ldots, f_k, \ldots$ are coefficients. Since $f(t)$ is a polynomial and thus smooth, we expand it, by Taylor's series, at the time instant n, leading to

$$f(t) = f(nT) + \frac{f^{(1)}(nT)}{1!}(t - nT)$$
$$+ \cdots + \frac{f^{(k)}(nT)}{k!}(t - nT)^k + \cdots. \tag{5}$$

Because we are studying a discrete time series and we need a recursive-type form, letting $t = (n+1)T$ and truncating at the order of K, we have

$$f(n+1) = f(n) + \frac{f^{(1)}(n)}{1!}T + \cdots + \frac{f^{(K)}(n)}{K!}T^K$$
$$= \sum_{k=0}^{K} \frac{f^{(k)}(n)}{k!}T^k = \sum_{k=0}^{K} \frac{T^k}{k!}f^{(k)}(n) \tag{6}$$

that is, the signal model in (2) could be alternatively given as

$$x(n+1) = \sum_{k=0}^{K} \frac{T^k}{k!}f^{(k)}(n) + s(n+1). \tag{7}$$

In (6) and (7), we use $f(n)$ to indicate $f(nT)$. This is just to follow the notation convention of the sampling theory. This means that the full form of (2) is $x(nT) = r(nT) + s(nT)$.

In order to estimate the mean function $f(n) = f^{(0)}(n)$ and its derivatives $f^{(k)}(n), k = 1, 2, \ldots, K$, we transfer the signal model (7) into the state space by defining the state vector

$$X(n) := \begin{bmatrix} X_0(n) \\ X_1(n) \\ X_2(n) \\ \cdots \\ X_K(n) \end{bmatrix} := \begin{bmatrix} f^{(0)}(n) \\ f^{(1)}(n) \\ f^{(2)}(n) \\ \cdots \\ f^{(K)}(n) \end{bmatrix}. \tag{8}$$

Therefore, we can rewrite (6) as the state equation

$$X(n+1) = \begin{bmatrix} 1 & T & \frac{T^2}{2} & \cdots & \frac{T^K}{K!} \\ 0 & 1 & T & \cdots & \frac{T^{K-1}}{(K-1)!} \\ 0 & 0 & 1 & \cdots & \frac{T^{K-2}}{(K-2)!} \\ \vdots & \vdots & \vdots & \ddots & \vdots \\ 0 & 0 & 0 & \cdots & 1 \end{bmatrix} X(n). \tag{9}$$

Besides, due to that we are observing the data stream of $x(n)$ [namely, the noised $r(n)$], we have the observation vector as

$$Y(n) := x(n) = f(n) + s(n) \tag{10}$$

that is, we have the following observation equation:

$$Y(n) := [1 \quad 0 \quad 0 \quad \cdots \quad 0]X(n) + V(n) \tag{11}$$

where $V(n)$ denotes the noise part $s(n)$.

By introducing the process noise $W(n)$, we have a state-space linear Gaussian–Markov system [12], [39]

$$\begin{cases} X(n+1) = \Phi X(n) + GW(n) \\ Y(n) = HX(n) + V(n) \end{cases} \tag{12}$$

where

$$\Phi := \begin{bmatrix} 1 & T & \frac{T^2}{2} & \cdots & \frac{T^K}{K!} \\ 0 & 1 & T & \cdots & \frac{T^{K-1}}{(K-1)!} \\ 0 & 0 & 1 & \cdots & \frac{T^{K-2}}{(K-2)!} \\ \vdots & \vdots & \vdots & \ddots & \vdots \\ 0 & 0 & 0 & \cdots & 1 \end{bmatrix} \tag{13}$$

$$H := [1 \quad 0 \quad 0 \quad \cdots \quad 0] \tag{14}$$

and

$$G := \begin{bmatrix} \frac{T^K}{K!} & \cdots & T & 1 \end{bmatrix}'. \tag{15}$$

In (15), $[\cdot]'$ denotes the transpose of a matrix.

The process noise $W(n)$ denotes the modeling errors, such as: 1) truncation error from (5)–(6) and 2) the innate impreciseness when using a polynomial $f(n)$ to approximate the true range $r(n)$. In (12), we treat $W(n)$ and $V(n)$ as independent and Gaussian random variables [12], [39], i.e., $E[W(n)W'(n)] = Q(n)$, $E[V(n)V'(n)] = R(n)$, $E[W(n)V'(n)] = 0$, $E[W(n)W'(n+k)] = 0$, and $E[V(n)V'(n+k)] = 0$, $\forall k \neq 0$. That is to say, $Q(n)$ denotes the covariance matrix of $W(n)$, while $R(n)$ denotes that of $V(n)$. In fact, $W(n)$, $V(n)$, $Q(n)$, $R(n)$, and $Y(n)$ are all 1×1 (i.e., scalars). We write them in boldface just to follow the notation conventions for a state-space model.

In summary, (7) and (12) give the models of a range measurement signal $x(n)$, satisfying the five requirements presented in the beginning of this section. The difference is that (12) is defined in the state space.

By using the signal model (7) and (12) for a range measurement $x(n)$, we do not explicitly take into account uncertainties

(e.g., outliers and dropouts) other than noises. The rationale is that an ideally **uncorrupted** range measurement time series contains only the true range $r(n)$ and the observation noise part $s(n)$. The noise part $s(n)$ is unavoidable since any sensor would, more or less, introduce random noises into the measured signal. Therefore, a range measurement signal that contains outliers/dropouts would **not fit** the model (7) and (12) well. It is this logic that makes possible the anomaly (i.e., outlier/dropout) detection for a time series. We only need to decide whether the measured range time series fit well the model (7) or (12) or not. If not, we take actions to correct the corresponding anomalies.

B. Choose the Model Order K

Usually, a larger K will cause less (polynomial) approximation error. However, in practice, there always exist uncertainties in measurements and the Runge phenomenon in the polynomial fitting. Thus, K should not be very large. By the authors' experiences from field tests and simulations, we suggest that K should be $2 \sim 5$. $K = 3$ and 4 are typical choices. More details about tuning K could be found in Section III.

C. Determine Q(n) and R(n)

Since $R(n)$ denotes the ranging error variance, i.e., the variance of the stationary noise process $s(n)$ in (2), it is easy to determine from the collected data in the field test. Note that the stationarity of $s(n)$ implies that $R(n) = R(n) = R$ is constant over time n. The first equality indicates that $R(n)$ is a scalar, while the second means that $R(n)$ is constant. Suppose that we have a part of collected range measurements $\mathcal{X}(n)$; we can use the block-data off-line polynomial regression method to extract its mean function $\Re(n)$. The subtraction gives the noise process $\mathcal{S}(n)$, i.e., $\mathcal{S}(n) := \mathcal{X}(n) - \Re(n)$. Thus, R is approximately given by the variance of the noise process $\mathcal{S}(n)$.

As for $Q(n)$, in practice, engineers may try different feasible $Q(n)$ to obtain different performances. According to [39], the value of $Q(n)$ actually adjusts our trust level toward the signal model that we use. Specifically, if we trust more of the observed data from the sensor, we choose to use relatively large values for $Q(n)$. However, if we trust more of the signal model, we choose to use relatively small values for $Q(n)$. According to authors' experiences, it is sufficient to let $Q(n)$ keep constant, i.e., $Q(n) = Q$, for many specific denoising and dropout/outlier correction problems. Therefore, $Q(n) = Q(n) = Q$ is also a 1×1 constant scalar, which is easy to tune after determining R. Fortunately, given R, there also exists an automatic method to determine Q [40].

D. Measurements Denoising and Outliers/Dropouts Correction

Since we now have the state-space signal model (12), we can use the model-based denoising methods. That is, we aim to estimate the true signal $f(n)$ and its derivatives $f^{(k)}(n), k = 1, 2, \ldots, K$. This can be done by applying the Kalman filter [39, Ch. 5.1] to the linear system (12).

During the denoising process, the outliers/dropouts can also be detected and corrected by the predict-and-replace method.
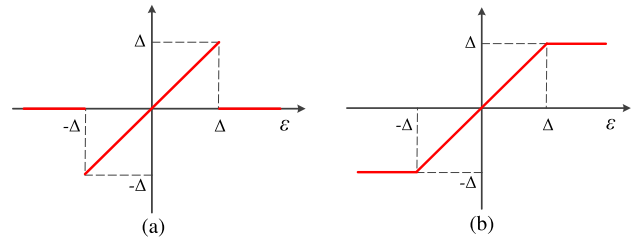

Fig. 3. Influence functions used to identify and remove/attenuate the outliers/dropouts. ϵ denotes the difference between the truly collected measurement and the predicted measurement. (a) Redescending influence function. (b) Monotonic influence function.

First, we mention that, if $f(n + 1) \gg \max\{f(n), f(n + 2)\}$, and $|f(n + 2) - f(n)| <$ a constant, i.e., if $f(n)$ and $f(n + 2)$ do not have very large difference, then we can identify $f(n + 1)$ as an outlier. If, alternatively, $f(n + 1) \ll \min\{f(n), f(n + 2)\}$, and $|f(n + 2) - f(n)| <$ a constant, $f(n + 1)$ is also an outlier. In this case, if simultaneously $f(n + 1) = 0$, $f(n + 1)$ is also a dropout. Second, we show the outlier/dropout identification and correction in our methodology. Suppose that the prediction of $x(n + 1)$ is $\hat{f}(n + 1)$. If the predicted value is far away from its noised measurement, we identify $x(n + 1)$ as an outlier/dropout. Mathematically, if

$$|x(n + 1) - \hat{f}(n + 1)| > \Delta \qquad (16)$$

$x(n + 1)$ is an outlier/dropout. Then, $x(n + 1)$ is replaced by $\hat{f}(n + 1)$. Δ is a preset threshold. Note that $\hat{f}(n + 1)$ is available from the Kalman filter. By doing so, we are actually utilizing the M-estimation techniques [16] with a redescending influence function shown in Fig. 3(a). Specifically, for example, if the error $\epsilon := x(n + 1) - \hat{f}(n + 1) > \Delta$, we replace $x(n + 1)$ with $\hat{f}(n + 1)$ so that $\epsilon = 0$. Another possible alternative for an influence function is the monotonic influence function shown in Fig. 3(b). It means, for example, that, if $\epsilon := x(n + 1) - \hat{f}(n + 1) > \Delta$, we replace $x(n + 1)$ with $\hat{f}(n + 1) + \Delta$ so that $\epsilon = \Delta$. As we can see, in the second case, we are not removing an outlier/dropout. Instead, we are attenuating an outlier/dropout. Other possible influence functions include Hampel's redescending function [18], the student's t redescending function [41], and so on. However, they still require one or more threshold parameter(s) (such as Δ in Fig. 3) to be carefully tuned.

In summary, we have Algorithm 1 to denoise and correct dropouts/outliers, in which the influence function in Fig. 3(a) is used to remove the dropouts/outliers. Other influence functions are also applicable. We do not cover the details.

According to [42, Th. 2], it is safe to set $\hat{X}(0) \leftarrow \mathbf{0}$ regardless of the true $X(0)$ because the estimated value $\hat{X}(n)$ converges to the true value $X(n)$ in the sense of unbiased minimum variance, as $n \to \infty$ for any finite $\hat{X}(0)$. For the rigorous and complete proofs, refer to [42].

Remark 2: Note that the difference-based method (e.g., $[x(n) - x(n - 1)]/T$) for estimating the derivative(s) of the mean function of a noised time series $x(n)$ is not reliable since the noises will be amplified by the difference operator.

Algorithm 1 Denoising and Outliers/Dropouts Correction

Definition: P as the state estimate co-variance in Kalman filter; I, $\mathbf{0}$ as an identity, null matrix with proper dimension; ∞ as a big number.

Notation: $\hat{f}(n)$ is the estimated/predicted value of $f(n)$; $\hat{X}(n)$ is the estimate of $X(n)$.

Initialization: $\infty \leftarrow 10^5$, $\hat{X}(0) \leftarrow \mathbf{0}$, $P(0) \leftarrow \infty \times I$, Q, R, Δ, $\hat{f}(1) \leftarrow x(1)$.

Remark: We can also let n starts from N instead of 1 and use the median of the first N measurements $x_{\text{median}(1:N)}$ to initialize $\hat{f}(N) \leftarrow x_{\text{median}(1:N)}$. This is a practical trick in case that outlier exists in the first several measurements. In the experiments section of this article, we use $N = 4$.

Input: $x(n)$, $n = 1, 2, 3, \ldots$ // or $n = N, N+1, N+2, \ldots$

1: **while** true **do**
2:      // Outliers/Dropouts Identification and Correction
3:      **if** $|\hat{f}(n) - x(n)| > \Delta$ **then**
4:          $x(n) \leftarrow \hat{f}(n)$ // Identified and Do Correction
5:      **end if**
6:
7:      // Estimate $\hat{f}^{(k)}(n)$ and Predict $\hat{f}(n+1)$
8:      $[\hat{X}(n), \hat{f}(n+1)]$ = Kalman_Filter$[x(n)]$
9:      $\hat{f}(n) \leftarrow \hat{X}_0(n)$
10:
11:      // Next round
12:      $n \leftarrow n + 1$
13: **end while**

Output: Noise attenuated and outliers/dropouts corrected ranging measurements $\hat{f}(n)$, and its derivatives $\hat{X}(n)$

Fig. 5. Leave-one-out method. Four sensors clustered into two classes by distances. (a) $\underline{\Delta}$ is larger than the given threshold so that the red point (right top) is not kept in the same class as the three rest blue/green (left bottom) points (four points not in the same class). (b) $\underline{\Delta}$ is smaller than the given threshold so that the blue point (left top) remains in the same class as the two green (right bottom) points (three points in the same class).
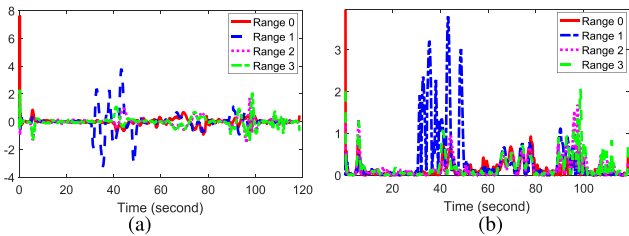

Fig. 4. Features of range measurements to distinguish Sensor 1 from others (see Fig. 2). (a) Second-order derivatives of the ranges in Fig. 2 (transformed measurements). (b) Absolute values of (a).

This fact is fundamental in the signal processing community, and we will not go through the details [43]. This is why we define the state variables and use the Kalman filter to recover $f(n)$ and its derivatives. $\qquad\square$

E. Anomaly Diagnosis and Sensor Selection

First, we use the problem in Fig. 2 as a running example to demonstrate the anomaly diagnosis and sensor selection method proposed in this article. In fact, the anomaly in Fig. 2 could be easily distinguished out by the derivatives of ranges (see Fig. 4). Therefore, the original time series classification problem (see Fig. 2) could be carried out in the feature space, namely, treating the second-order derivative of a range
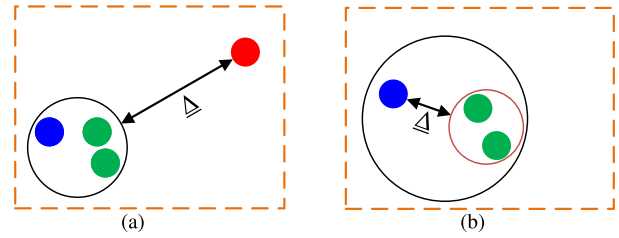
time series as its feature. Comparing Fig. 4 with Fig. 2, the transformed four time series are easier to classify. It is obvious that, during the times around 30∼50 s, Sensor 1 significantly stands out in the feature space illustrated in Fig. 4. Now, the sensor selection problem is transformed into a time series classification problem [44]. We could, respectively, apply the l_p-norm to calculate the distance between any two range time-series measurements and then use the distance-based clustering method, such as k-means in the machine learning community to group the four range series. Suppose that the length of the two range time series $x_1(n)$ and $x_2(n)$ is L; the distance between $x_1(n)$ and $x_2(n)$ is given as $D_{x_1,x_2} = [\sum_{n=0}^{L} |x_1(n) - x_2(n)|^p]^{1/p}$. Typical choices for p in practice, according to [44] and also authors' experiences, are $p = 1$ or $p = 2$. However, the time series range measurements are obtained in the stream, not in block, meaning that we cannot apply the L-length l_p-norm to the whole $x_1(n)$ and $x_2(n)$ *post hoc*. Therefore, in practice, we apply the L-length l_p-norm to successive subsequences of, for example, $x_1(n)$, i.e., the subsequences $\{x_1(1), x_1(2), \ldots, x_1(L)\}$, $\{x_1(2), x_1(3), \ldots, x_1(L+1)\}$, $\{x_1(3), x_1(4), \ldots, x_1(L+2)\}, \ldots, \{x_1(m), x_1(m+1), \ldots, x_1(L+m-1)\}$, and so on. Whenever one of the sensors is significantly away from the rest three sensors at one time instant, the sensor should be excluded from the functioning sensor bank at this time instant. Following this logic, UWB Sensor 1 in Fig. 2 must be excluded. When there are many anchors available for positioning, there may exist more than one unreliable sensor. Therefore, we should continuously apply this "leave-one-out" idea to remove the dysfunctional sensors, one by one, until there are at least four sensors left for 3-D positioning or at least three sensors left for 2-D positioning. Fig. 5 illustrates the idea of the leave-one-out method, in which $\underline{\Delta}$ denotes the distance from the removed point to the circle containing the rest points. The center of the circle is the point obtained from averaging the children points, and the radius is the largest distance from the center to the children points.

Second, in Algorithm 2, we, summarize the proposed sensor selection method.

Remark 3: The proposed sensor selection method in this section is *ad hoc* for one type of nonspecific UWB ranging anomalies shown in Fig. 2, which may occur sometimes in some environments. Thus, we are not claiming the generality

---

Algorithm 2 Sensor Selection

Definition: L: Length of the sub-sequence. Ω: Threshold to determine whether a sensor is problematic or not (i.e., threshold of $\underline{\Delta}$). M: Number of anchors available (i.e., number of range time series). $\hat{X}_k^m(n)$: Estimated k^{th}-order derivative (e.g., $k = 2$) of the range time series from m^{th} anchor. Dist(x, y): Calculate the distance of two time series x and y based on l_p norm. $X(S:E)$: A sub-sequence of X with indices starting from S and ending at E. $\emptyset$: Empty set. $\bar{i}$: Index of the sensor removed by the leave-one-out method.

Reservation: $\mathcal{I}(n)$: the index set of the malfunctioning sensors at the time instant n.

Initialization: $\infty \leftarrow 10^5$, $\underline{\Delta} \leftarrow \infty$, k, L, Ω.

External: Call Algorithm 1 to obtain $\hat{X}^m(n)$ for the range time series from the mth anchor. cf. $\hat{X}(n)$ and $\hat{X}_k(n)$ in (8)

Input: $\hat{X}_k^m(n)$, $m = 1, 2, 3, \ldots, M$, $n = L+1, L+2, \ldots$
1: **while** true **do**
2:     // Get the distances between $\hat{X}_k^i(n)$ and $\hat{X}_k^j(n)$
3:     **for** $i = 1$ to M **do**
4:         **for** $j = 1$ to M **do**
5:             $S \leftarrow n - L$
6:             $E \leftarrow n - 1$
7:             $D(i, j) = \text{Dist}\{\hat{X}_k^i(S:E), \hat{X}_k^j(S:E)\}$
8:         **end for**
9:     **end for**
10:
11:     // Do leave-one-out clustering and sensor selection
12:     $\mathcal{I}(n) \leftarrow \emptyset$
13:     **while** $\exists$ more than least-required no. of anchors **do**
14:         $\bar{i} \leftarrow \text{Leave\_One\_Out}(D)$
15:         Calculate $\underline{\Delta}$ // See Fig. 5
16:
17:         // Sensor Selection
18:         **if** $\underline{\Delta} > \Omega$ **then**
19:             $\mathcal{I}(n) \leftarrow \mathcal{I}(n) \bigcup \bar{i}$ // This is a morbid sensor
20:             **continue while**
21:         **else**
22:             **break while**
23:         **end if**
24:     **end while**
25:
26:     // Next round
27:     $n \leftarrow n + 1$
28: **end while**
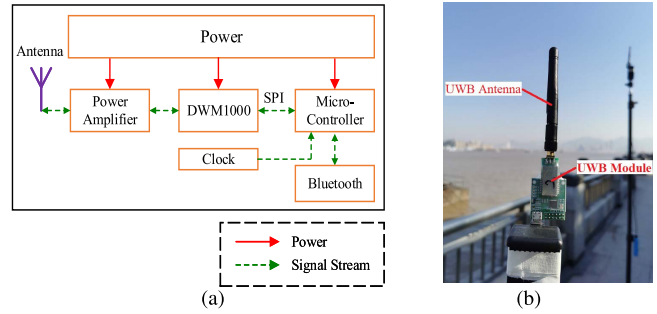**Output**: The morbid sensor set $\mathcal{I}(n)$ at each time instant n

Fig. 6. UWB ranging circuit. Bluetooth is used to transmit the measured range to the remote server, e.g., a computer to collect range data. (a) Topology. (b) Real.
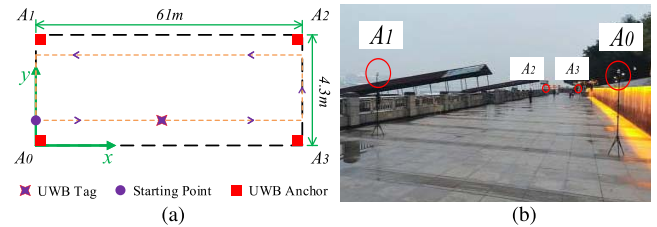

Fig. 7. UWB test field with a dimension of 61×4.3 m^2. The orange dotted rectangular trajectory (starting from the purple-filled circle) is used to collect the ranging measurements displayed in Fig. 1. A0, A1, A2, and A3 are UWB anchors. The origin of the coordinate is fixed on A0. (a) Test field (topology). (b) Test field (real).

of the proposed method in any situation. If engineers encountered other types of specific or nonspecific anomalies discussed in other related studies [27], [32], [33], [37], they could refer to corresponding works for a more appropriate method. □

III. EXPERIMENT RESULTS AND ANALYSES

All the source data and codes are available online at GitHub: https://github.com/Spratm-Asleaf/Range-Correction.

A. Real Field Test

1) Settings: The UWB module embedded in our ranging circuit is DWM1000 produced by DECAWAVE (https://www.decawave.com/product/dw1000-radio-ic/). We integrated together with the UWB module, UWB antenna, power, power amplifier circuit, clock, communication buses [i.e., serial peripheral interface (SPI)], microcontroller (i.e., STM32F103C8T6), and Bluetooth to build the ranging circuit (see Fig. 6). The ranging protocol is the symmetric-double-sided two-way time-of-arrival (SDS-TW-TOA) based on the IEEE Standard 802.15.4a [45].

The UWB testing field that we were working in to collect the data in Fig. 1 is illustrated in Fig. 7. The trajectory starts from the purple-filled circle and is along the orange-dotted rectangular. We walked along the rectangular trajectory for almost two rounds. Fig. 1(a) shows the ranging measurements from the A3 while Fig. 1(b) from the A0. The sampling time is $T = 0.1$ s. The variance of ranging errors is $R = (0.05/3)^2$ (from the real data, $3\sigma = 5$ cm, and σ is the standard deviation). For details of getting R, see Section II-C.

2) Performances of Denoising and Outliers/Dropouts Correction: In this first experiment, as a demonstration, the parameters are set as $K = 3$, $Q = 0.01^2$, and $\Delta = 2.0$. Q and Δ are tunable parameters and determined case-by-case. In Fig. 8, we display the denoising performance of the proposed method compared with that of the traditional exponential smoothing method. In Fig. 9, we show the performances of denoising and outliers/dropouts correction using Algorithm 1. The data used are the same as in Figs. 1 and 7. From Fig. 9, we can see that the proposed method can effectively
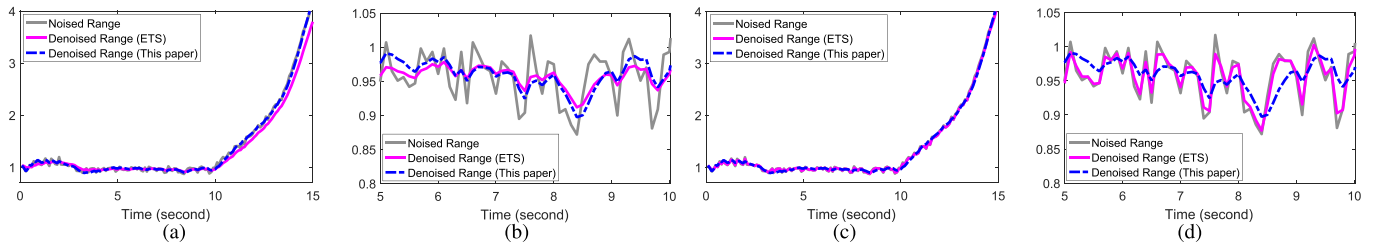
Fig. 8.　Denoising performances of the traditional signal-model-free exponential smoothing (ETS) method and the proposed method when the target is in static (i.e., time from 0 to 10 s) and in high-maneuvering (i.e., time from 10 to 15 s). (a) and (b) ETS has large biases but small fluctuations. (c) and (d) ETS has small biases but large fluctuations. We can see that, if the ETS has small fluctuation when in static, it must have large biases when in high-maneuvering [see (a) and (b)], and vice versa [see (c) and (d)]. That is to say, the traditional denoising method either has large fluctuations or has large biases. This dilemma has to be met, and we cannot detour. However, the proposed method can balance the two performances. The unit in the y-axis is meter. The data are from $A0$. (a) ETS parameter $= 0.25$. (b) ETS parameter $= 0.25$ (closeup). (c) ETS parameter $= 0.75$. (d) ETS parameter $= 0.75$ (closeup).
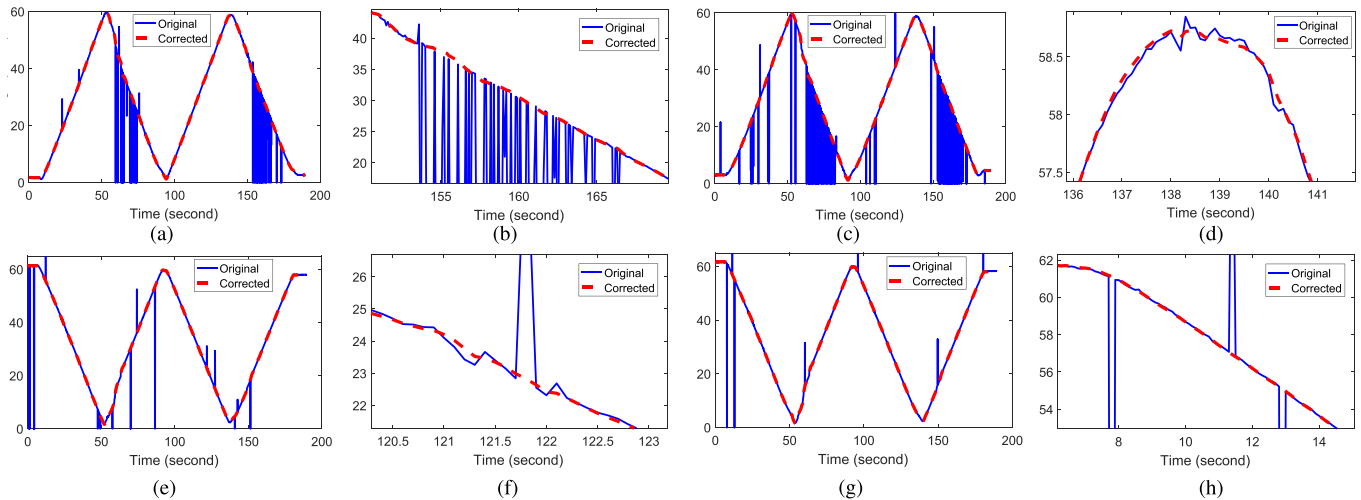

Fig. 9.　Performances of denoising and outliers/dropouts correction using Algorithm 1. The unit in the y-axis is meter. (a) Measurements from $A0$. (b) Closeup of (a). (c) Measurements from $A1$. (d) Closeup of (c). (e) Measurements from $A2$. (f) Closeup of (e). (g) Measurements from $A3$. (h) Closeup of (g).

eliminate the fluctuations in the ranging measurements [see Fig. 9(d) and (f)] and identify and correct the outliers/dropouts [see Fig. 9(f) and (h)], even when the outliers/dropouts are very dense [see Fig. 9(b) and (c)].

3) Comparison Experiments: In this section, we compare the algorithm performance with some of the existing representative methods, over the range measurements from $A1$. The Δ and Q keep unchanged as 2.0 and 0.01^2, respectively.

First, we compare with one statistical outlier-correction method introduced in [24] (i.e., one-sided median method). In the one-sided median method, the parameters are set as $\kappa = 10$ and $\tilde{\tau} = 8.0$ (see [24, Sec. 3.2]). If we set $K = 1$, $K = 2$, $K = 3$, and $K = 4$, respectively, we have the results in Fig. 10. As we can see, all methods could roughly behave well, besides the one-sided median method although it is already equipped with the tuned parameters (i.e., κ and $\tilde{\tau}$) that have the best performances. Furthermore, when outliers and dropouts are dense, larger K will, on the contrary, lead to large errors [see times around $155 \sim 160$ in Fig. 10(b) and (c)]. On the other hand, if K is extremely small, e.g., when $K = 1$, large errors would also be introduced. Therefore, in this case, Algorithm 1 with $K = 2$ or $K = 3$ basically gives satisfactory solutions.
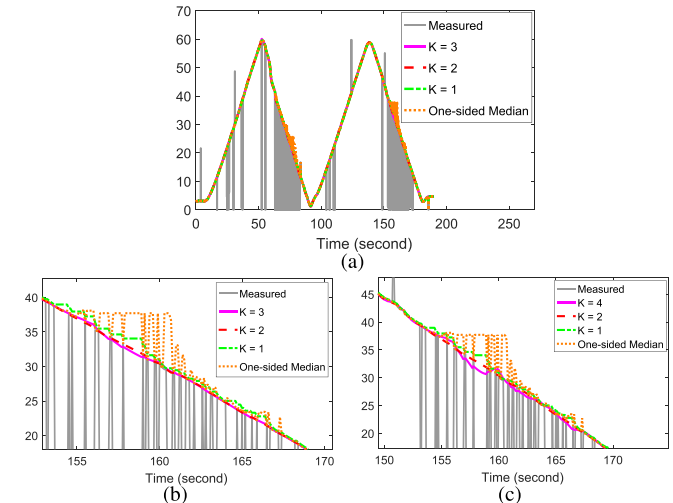

Fig. 10.　Performances of denoising and outliers/dropouts correction using Algorithm 1 with different K's over the real data (measurements from $A1$). When $K = 4$, there is a significant vibration in (b) during times around $155 \sim 160$. (a) For $K = 3$, it does not have this phenomenon. (a) For $K = 1, 2$, and 3. (b) Closeup of (a). (c) Closeup when $K = 1, 2$, and 4.

Second, we implement a robust method introduced in [22] to compare the performances with Algorithm 1 ($K = 3$). Q and Δ remain unchanged as before. The results are
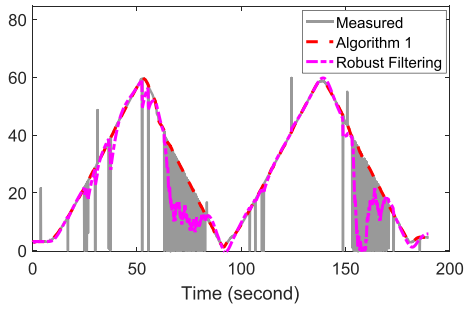
Fig. 11. Comparison experiments between Algorithm 1 and a robust filtering [22]. The robust filter cannot guarantee a convergent solution for the range measurements with dense outliers.
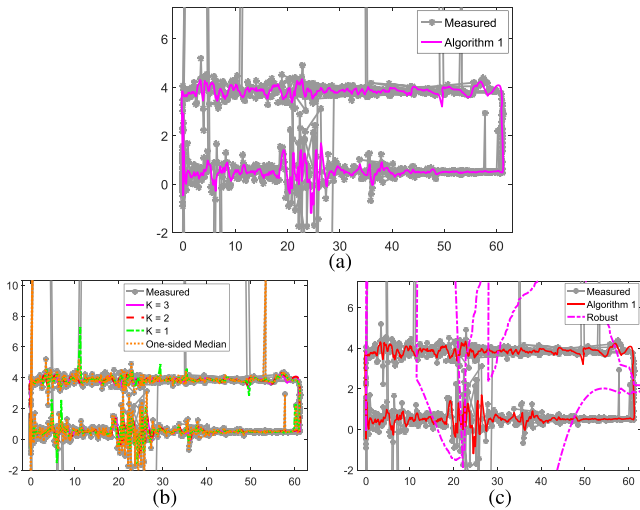

Fig. 12. Positioning results [see Fig. 7(a)]. (a) Positioning results are obtained using the original range measurements and the corrected ranges with Algorithm 1 with $K = 3$. (b) Positioning results are obtained using different K's and the one-sided median. (c) Positioning results are obtained using $K = 3$ and the robust method.
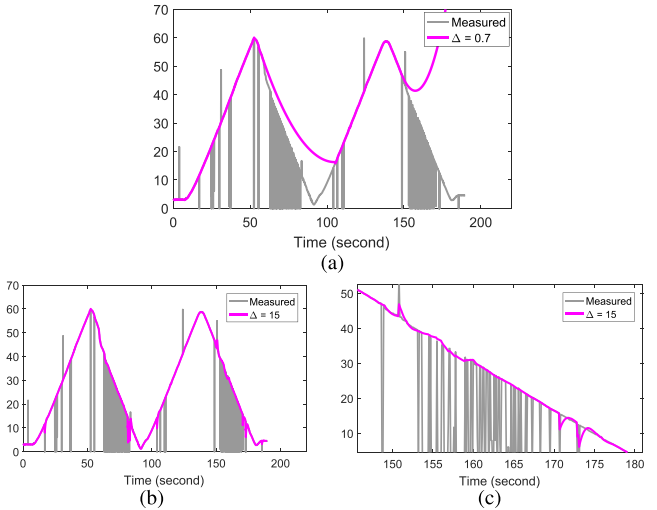

Fig. 13. Threshold Δ of Algorithm 1 matters a lot (see Fig. 10 where $\Delta = 2$). (a) Small $\Delta = 0.7$. (b) Big $\Delta = 15$. (c) Closeup of (b).
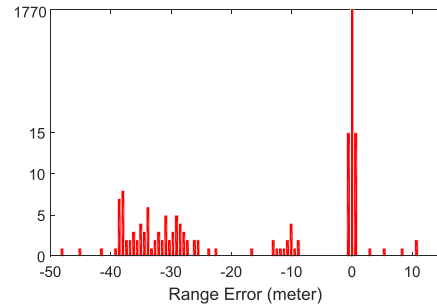

Fig. 14. Range error histogram of A_0. Most of errors are around zero. However, there is a significant sidelobe in the error distribution.

shown in Fig. 11. As we can see from Fig. 11, the robust filter even cannot guarantee a convergent solution for the range measurements with dense outliers (see times during $50 \sim 100$) although there are relatively effective for sparse outliers/dropouts (see times during $100 \sim 150$).

4) Positioning Results: Then, we implement a multiple-anchor positioning method in [29] to obtain the real-time position of the UWB receiver, in which the ranges are squared and subtracted so that the range-based TOA problem is transformed into a pseudo-TDOA problem (see Fig. 12). As we can see from Fig. 12(a), without correcting ranges, the positioning results with the original range measurements are really unsatisfactory. There are severe noises and outliers. However, if we use the corrected ranges from Algorithm 1 with $K = 3$, we can obtain noticeably better positioning results. In contrast, Algorithm 1 with $K = 1$ and the one-sided median method are not satisfactory because there still have some outliers in the positioning results. The robust method even diverges (i.e., it even performs worse than the raw ranges).

5) Performances of Outlier/Dropout Treatment Under Different Δ's: In fact, the threshold Δ in Algorithm 1 matters a lot. When it is too small, the algorithm cannot be guaranteed to converge; when too large, significant errors would exist. This is easy to understand from the logic of the algorithm. Intuitively, see Fig. 13. Other parameters and the data used are the same as those in Fig. 10 (namely, $K = 3$ and $Q = 0.01^2$). Therefore, at present, we can only carefully choose proper Δ for each specific problem. We expect an adaptive/automatic tuning method for it in the future.

6) Range Error Histogram: If we use the corrected ranges from Algorithm 1 with $K = 3$ as the true ranges, we can obtain the ranging errors of A_0. The histogram is shown in Fig. 14. As we can see, it is a multiple-modal distribution that is far away from a Gaussian distribution or a student's t distribution. Therefore, statistical outlier-rejection methods based on the assumption of a student's t distribution [46] or on a skew Gaussian-gamma mixture distribution [47] are not preferable for our range-correction problem.

7) Mean Square Error: Since it is hard to obtain the exactly true ranges against the time of a moving target, we cannot calculate the mean square error (mse) between the corrected range time series and the true range time series. Even though the moving target can exactly follow a fixed straight-line trajectory, different moving (but unobservable) speeds generate different range time series (see Fig. 15). For the same reason,
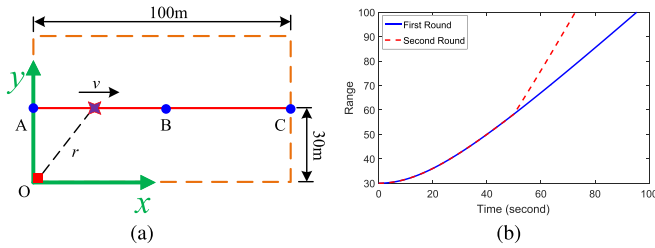
Fig. 15. True range time series r depends on the true but ***unobservable*** moving speed v. (a) Target is moving from A to C via B (B is the middle point of A and C). In the first round, the true speed v is fixed as 1 m/s, while, in the second round, the true speed from A to B is 1 m/s but from B to C is 2 m/s. (b) Two range time series associated with (a).
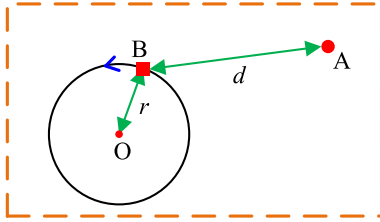

Fig. 16. Simulated field. We are investigating the range between anchor A and rover B. Rover B is moving along the circle centered at O, counterclockwise.

we cannot obtain mse between the true trajectory and the calculated trajectory because we also do not know the true position (against time) of the moving target. Thus, another experiment is conducted over a simulated dataset where the ground truth of range-time data pairs is available so that we can calculate the corresponding mses.

B. Simulated Test

1) Setting: Suppose that the simulated ranges are from a circle trajectory in one testing field (see Fig. 16). Therefore, the square of the range time series must be a sine function. Note that, if the position of O is $[x_1, y_1]$ and that of A is $[x_0, y_0]$, we have the range time series as

$$
\begin{aligned}
d &= \sqrt{[x_1 + r\cos\theta - x_0]^2 + [y_1 + r\sin\theta - y_0]^2} \\
&= \sqrt{\alpha + \beta\cos\theta + \gamma\,\sin\theta} \\
&= \sqrt{\alpha + \xi\sin\phi}
\end{aligned}
\tag{17}
$$

where θ and ϕ are independent variables of d and constant coefficients α, β, γ, and ξ are defined by x_1, y_1, x_0, y_0, and r. Therefore, d^2 is a sine function.

Without loss of generality, we suppose that the interested range time series is

$$
x(n) = \sqrt{401 + 400\sin(0.1 \times 0.1 \times n)} + 0.1\,\mathrm{GW}(n)
$$

that is, the sampling time is still 0.1 s (recall that $t = Tn$), where $\mathrm{GW}(n)$ denotes a Gaussian white stochastic process with the mean of 0 and the variance of 1. In this experiment, in order to noticeably see the performance of the proposed algorithm, we improve the standard deviation of the Gaussian white process to 0.1 m (instead of the small 0.05 m/3 in the real data). Therefore, there is a coefficient 0.1 before
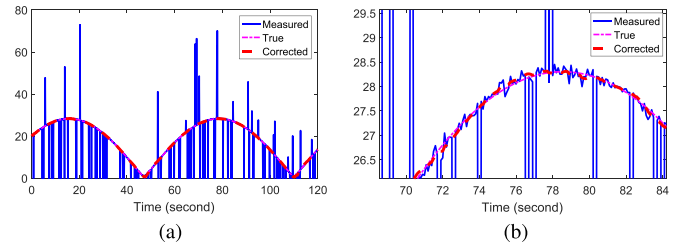

Fig. 17. Performances of denoising and outliers/dropouts correction using Algorithm 1 with the simulated data. (a) Simulation results. (b) Closeup of (a).
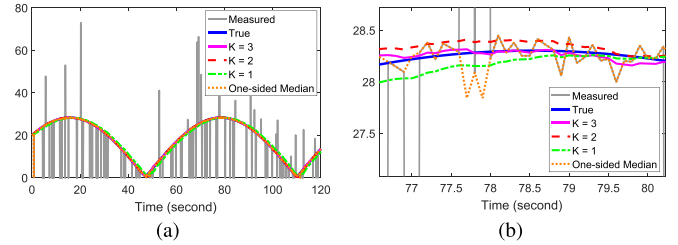

Fig. 18. Comparison experiments between Algorithm 1 and the one-sided median method with the simulated data. (a) Simulation results. (b) Closeup of (a).

TABLE I
MSE RESULTS OF THE SIMULATED EXPERIMENT

	Non-denoised and Non-corrected	One-Sided Median	$K = 3$
MSE	44.1605	0.7446	0.0204
	$K = 2$	$K = 1$	Robust
MSE	0.0458	1.0468	13.2256

Note: Robust method is corresponding to Fig. 19, while other methods are to Fig. 18.

$\mathrm{GW}(n)$. The simulation runs max $(n) = 1200$ steps. Besides, we randomly add 20 outliers and 100 dropouts in $x(n)$.

2) Performances of Denoising and Outliers/Dropouts Correction: In this case, $R = 0.1^2$. The parameters Δ and Q keep unchanged as 2.0 and 0.01^2, respectively. We implement Algorithm 1 with $K = 1, 2$, and 3 and the one-sided median method in [24]. In the one-sided median method, the parameters are set as $\kappa = 10$ and $\tilde{\tau} = 2.0$ (see [24, Sec. 3.2]). We have the results in Figs. 17 and 18.

Also, we give the mse, compared to the true ranges (because, in this experiment, we know the true ranges against time), of the denoised/corrected range measurements with different methods, and nondenoised and noncorrected range measurements, respectively, in Table I. We can see that all these methods are effective in denoising and removing the outliers/dropouts. However, Algorithm 1 with $K = 3$ outperforms the others. This is because Algorithm 1 with $K = 1$ and 2 introduces the biases when denoising a quick-changing signal [like the exponential smoothing method does (see Fig. 8)], while the one-sided median method has no innately designed mechanism to denoise.

Besides, for the comparison purpose, we also implement the robust filtering method introduced in [22]. The result is
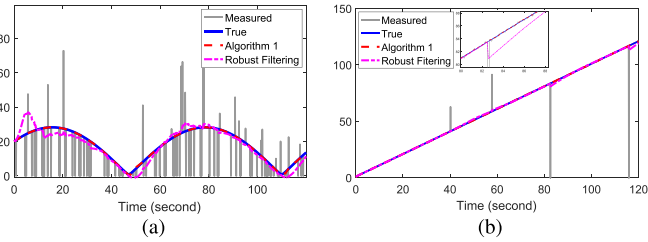
Fig. 19. Comparison experiments between Algorithm 1 and the robust filtering [22]. (a) Sine range time series. (b) $x(n) = 1 + 0.1n + 0.1GW(n)$; time series is slow-changing, and outliers/dropouts are sparse.

TABLE II
PURE DENOISING PERFORMANCES UNDER DIFFERENT K'S

	$K = 1$	$K = 2$	$K = 3$	$K = 4$
MSE ($Q = 0.01^2$)	33.2006	1.6159	0.2633	**0.1954**
MSE ($Q = 0.05^2$)	3.1206	0.1912	**0.1678**	0.2160

given in Fig. 19(a). As we can see from Fig. 19, although the robust filtering method in [22] can withstand the uncertainties to some extent, it also denies the quick-changing pattern of a ranging time series. That is, it introduces the biases when the time series is quick-changing because the robust filtering treats the quick-changing part of a time series as uncertainty and takes effort to revolt it. This is an innate drawback of all robust filtering strategies. Contrarily, when the time series is slow-changing and outliers/dropouts are sparse, the robust filtering method could have a relatively desired performance. See Fig. 19(b), in which $x(n) = 1 + 0.1n + 0.1GW(n)$. However, the imperfection of removing outliers/dropouts still exists; for example, see the subfigure around $t = 82.5$ s of Fig. 19(b), in which, although the outlier is to some degree suppressed, a jitter still appears.

C. Performances of Pure Denoising Under Different K's

In order to compare the pure denoising performances, we compare Algorithm 1 with different K's for range measurement without outliers. This time, let us consider $x(n) = (401 + 400 \sin(0.1 \times 0.1 \times n))^{1/2} + GW(n)$ with the sampling time of 0.1 s but the variance of $GW(n)$ is, instead, larger (i.e., 1 m). We implement Algorithm 1 with $K = 1$, $K = 2$, $K = 3$, and $K = 4$, respectively. Besides, we set $R = 1^2$ and $\Delta = 2.0$. As we can see form Table II, a relatively larger K is likely to lead to less estimation errors because the model with a smaller K cannot track the quick-changing pattern of a range time series [i.e., having large tracking bias. (see Fig. 8)]. However, this is conditioned on how to select Q. Sometimes, the model with an extremely large K would, in turn, be sensitive to noises, and it would introduce larger mse.

D. Sensor Selection

We use Algorithm 2 to select the malfunctioning sensor in Fig. 4. The parameters are set as $L = 50$ and $\Omega = 15$. We have the result in Fig. 20. The result is consistent with
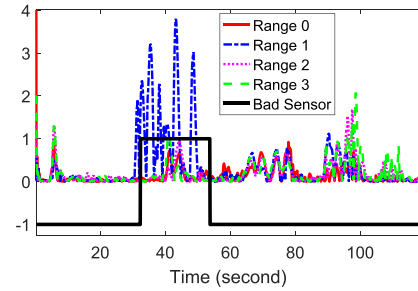

Fig. 20. Sensor selection result using Algorithm 2 over Fig. 4. If the value of "Bad Sensor" is -1, there is no bad sensor at present. The value is 1 means that Sensor 1 is identified as a diseased sensor.

our expectation that Sensor 1 is morbid during the time period [32.3, 53.8]. We note that there is a small time delay in the result. This is because we use the window length of 50. However, the strict tuning methods for L and Ω are open. At present, we can only suggest that the authors should try proper values for their own specific problems.

E. Highlights on Experiments Results

Experiments show that the proposed method is powerful in tracking the true information of a range time series (i.e., no bias), in suppressing the random noises, identifying and correcting the outliers/dropouts, and reporting one kind of nonspecific anomalies in the range measurements. The main results from the experiments are given as follows.

1) The typical choices for K are 2, 3, and 4. The model with both very large and very small K is likely to have large filtering errors. Specifically, a larger K is suitable to track the quick-changing pattern of the range time series, which will help lower the filtering biases. However, when outliers/dropouts are very severe/dense, the model with a larger K is vulnerable to them as well. In contrast, a smaller K is suitable to track the slow-changing pattern of the range time series, which will also help withstand the (dense) outliers/dropouts. However, when outliers/dropouts are relatively slight/sparse, a smaller K is likely to introduce larger filtering biases when tracking a quick-changing time series. In particular, $K = 2$ and 3 are suitable for range measurements with dense outliers/dropouts, while $K = 4$ is proper for range measurements with sparse (or without) outliers/dropouts.

2) The tuning method of the threshold Δ in Algorithm 1 is open. A too small value is likely to make the algorithm divergent, while a too large value may lead to significant jerks, i.e., vulnerable to severe uncertainties [see Fig. 13(c)]. Besides, the tuning method of the parameters L and Ω in Algorithm 2 is also empirical. At present, the authors' can only suggest that readers try appropriate values for their specific problems.

3) As stated in Remark 3, the sensor selection method that we presented only provides one possible alternative for engineers, asserting no dominating position over other participant methods in any situation.

4) When range measurements are reliable for sure, Algorithm 1 could be reset and restarted. If the range measurements were not informative in the past, the predictions for the future would be questionable. Thus, when the users believe that reliable range measurements come again, they can clean the bad memory of Algorithm 1.

IV. Conclusion

This article introduces a new state-space stochastic-process model for a nonstationary stochastic time series and identifies the derivatives of its mean function as state variables. The model has benefits as follows.

1) It equips a general time series with a state-space model that enables the use of the model-based signal processing methods.
2) It is a recursive-type time series that is workable for sequential data.
3) It can exactly track the quick—but smooth—changing time series due to the participation of the derivatives.
4) It can tell apart a sharp-changing subsequence of a time series as an anomaly.
5) It coincides with the standard form (i.e., a linear Gaussian–Markov model in the state space) required in the Kalman filter settings so that the defined states can be estimated by the Kalman filter.

The proposed outlier/dropout treatment method is functionally complementary to the traditional NLOS/LOS error elimination methods in the sense that the following holds.

1) It can efficiently filter the random noises.
2) It can handle the dropouts and signal-processor-related outliers that cannot be addressed by the traditional NLOS/LOS error elimination methods.
3) It can identify one sort of nonspecific sensor anomaly (see Fig. 2) that cannot be detected by the traditional NLOS/LOS error elimination techniques and existing sensor selection methods.

References

[1] S. Gezici and H. V. Poor, "Position estimation via ultra-wide-band signals," *Proc. IEEE*, vol. 97, no. 2, pp. 386–403, Feb. 2009.

[2] A. Alarifi *et al.*, "Ultra wideband indoor positioning technologies: Analysis and recent advances," *Sensors*, vol. 16, no. 5, p. 707, May 2016.

[3] V. Savic, J. Ferrer-Coll, P. Angskog, J. Chilo, P. Stenumgaard, and E. G. Larsson, "Measurement analysis and channel modeling for TOA-based ranging in tunnels," *IEEE Trans. Wireless Commun.*, vol. 14, no. 1, pp. 456–467, Jan. 2015.

[4] T. Risset, C. Goursaud, X. Brun, K. Marquet, and F. Meyer, "UWB ranging for rapid movements," in *Proc. Int. Conf. Indoor Positioning Indoor Navigat. (IPIN)*, Sep. 2018, pp. 1–8.

[5] H. Perakis and V. Gikas, "Evaluation of range error calibration models for indoor UWB positioning applications," in *Proc. Int. Conf. Indoor Positioning Indoor Navigat. (IPIN)*, Sep. 2018, pp. 206–212.

[6] L. Cong and W. Zhuang, "Nonline-of-sight error mitigation in mobile location," *IEEE Trans. Wireless Commun.*, vol. 4, no. 2, pp. 560–573, Mar. 2005.

[7] H. Wymeersch, S. Marano, W. M. Gifford, and M. Z. Win, "A machine learning approach to ranging error mitigation for UWB localization," *IEEE Trans. Commun.*, vol. 60, no. 6, pp. 1719–1728, Jun. 2012.

[8] T. Aguilera, F. J. Alvarez, D. Gualda, J. M. Villadangos, A. Hernandez, and J. Urena, "Multipath compensation algorithm for TDMA-based ultrasonic local positioning systems," *IEEE Trans. Instrum. Meas.*, vol. 67, no. 5, pp. 984–991, May 2018.

[9] V. Savic, E. G. Larsson, J. Ferrer-Coll, and P. Stenumgaard, "Kernel methods for accurate UWB-based ranging with reduced complexity," *IEEE Trans. Wireless Commun.*, vol. 15, no. 3, pp. 1783–1793, Mar. 2016.

[10] S. Y. Cho, "Two-step calibration for UWB-based indoor positioning system and positioning filter considering channel common bias," *Meas. Sci. Technol.*, vol. 30, no. 2, Feb. 2019, Art. no. 025003.

[11] J. Khodjaev, Y. Park, and A. S. Malik, "Survey of NLOS identification and error mitigation problems in UWB-based positioning algorithms for dense environments," *Ann. Telecommun.*, vol. 65, nos. 5–6, pp. 301–311, Jun. 2010.

[12] H. H. Afshari, S. A. Gadsden, and S. Habibi, "Gaussian filters for parameter and state estimation: A general review of theory and recent trends," *Signal Process.*, vol. 135, pp. 218–238, Jun. 2017.

[13] P. S. Diniz, E. A. Da Silva, and S. L. Netto, *Digital Signal Processing: System Analysis and Design*. Cambridge, U.K.: Cambridge Univ. Press, 2010.

[14] G. E. Box, G. M. Jenkins, G. C. Reinsel, and G. M. Ljung, *Time Series Analysis: Forecasting and Control*. Hoboken, NJ, USA: Hoboken, NJ, USA: Wiley, 2015.

[15] Q. Zhai and Z.-S. Ye, "Robust degradation analysis with non-Gaussian measurement errors," *IEEE Trans. Instrum. Meas.*, vol. 66, no. 11, pp. 2803–2812, Nov. 2017.

[16] A. M. Zoubir, V. Koivunen, Y. Chakhchoukh, and M. Muma, "Robust estimation in signal processing: A tutorial-style treatment of fundamental concepts," *IEEE Signal Process. Mag.*, vol. 29, no. 4, pp. 61–80, Jul. 2012.

[17] S. Sun, T. Tian, and H. Lin, "Optimal linear estimators for systems with finite-step correlated noises and packet dropout compensations," *IEEE Trans. Signal Process.*, vol. 64, no. 21, pp. 5672–5681, Nov. 2016.

[18] L. Chang and K. Li, "Unified form for the robust Gaussian information filtering based on M-estimate," *IEEE Signal Process. Lett.*, vol. 24, no. 4, pp. 412–416, Apr. 2017.

[19] H. Wang, H. Li, J. Fang, and H. Wang, "Robust Gaussian Kalman filter with outlier detection," *IEEE Signal Process. Lett.*, vol. 25, no. 8, pp. 1236–1240, Aug. 2018.

[20] C. Masreliez and R. Martin, "Robust Bayesian estimation for the linear model and robustifying the Kalman filter," *IEEE Trans. Autom. Control*, vol. AC-22, no. 3, pp. 361–371, Jun. 1977.

[21] A. Alessandri and L. Zaccarian, "Stubborn state observers for linear time-invariant systems," *Automatica*, vol. 88, pp. 1–9, Feb. 2018.

[22] Z. Li, Y. Yao, J. Wang, and J. Gao, "Application of improved robust Kalman filter in data fusion for PPP/INS tightly coupled positioning system," *Metrol. Meas. Syst.*, vol. 24, no. 2, pp. 289–301, Jun. 2017.

[23] Y. S. Shmaliy, F. Lehmann, S. Zhao, and C. K. Ahn, "Comparing robustness of the Kalman, H_∞, and UFIR filters," *IEEE Trans. Signal Process.*, vol. 66, no. 13, pp. 3447–3458, May 2018.

[24] S. Basu and M. Meckesheimer, "Automatic outlier detection for time series: An application to sensor data," *Knowl. Inf. Syst.*, vol. 11, no. 2, pp. 137–154, Feb. 2007.

[25] Y. He, Y. Peng, S. Wang, and D. Liu, "ADMOST: UAV flight data anomaly detection and mitigation via online subspace tracking," *IEEE Trans. Instrum. Meas.*, vol. 68, no. 4, pp. 1035–1044, Apr. 2019.

[26] M. Braei and S. Wagner, "Anomaly detection in univariate time-series: A survey on the state-of-the-art," 2020, *arXiv:2004.00433*. [Online]. Available: https://arxiv.org/abs/2004.00433

[27] J. S. Picard and A. J. Weiss, "Bounds on the number of identifiable outliers in source localization by linear programming," *IEEE Trans. Signal Process.*, vol. 58, no. 5, pp. 2884–2895, May 2010.

[28] M. Compagnoni *et al.*, "A geometrical–statistical approach to outlier removal for TDOA measurements," *IEEE Trans. Signal Process.*, vol. 65, no. 15, pp. 3960–3975, Aug. 2017.

[29] S. Cao, X. Chen, X. Zhang, and X. Chen, "Combined weighted method for TDOA-based localization," *IEEE Trans. Instrum. Meas.*, vol. 69, no. 5, pp. 1962–1971, May 2020.

[30] L. Lin, H. C. So, F. K. W. Chan, Y. T. Chan, and K. C. Ho, "A new constrained weighted least squares algorithm for TDOA-based localization," *Signal Process.*, vol. 93, no. 11, pp. 2872–2878, Nov. 2013.

[31] T. V. Nguyen, Y. Jeong, H. Shin, and M. Z. Win, "Least square cooperative localization," *IEEE Trans. Veh. Technol.*, vol. 64, no. 4, pp. 1318–1330, Apr. 2015.

[32] N. Wu, Y. Xiong, H. Wang, and J. Kuang, "A performance limit of TOA-based location-aware wireless networks with ranging outliers," *IEEE Commun. Lett.*, vol. 19, no. 8, pp. 1414–1417, Aug. 2015.

[33] H. Ozkan, F. Ozkan, and S. S. Kozat, "Online anomaly detection under Markov statistics with controllable type-I error," *IEEE Trans. Signal Process.*, vol. 64, no. 6, pp. 1435–1445, Mar. 2016.

[34] S. Liu, S. P. Chepuri, M. Fardad, E. Masazade, G. Leus, and P. K. Varshney, "Sensor selection for estimation with correlated measurement noise," *IEEE Trans. Signal Process.*, vol. 64, no. 13, pp. 3509–3522, Jul. 2016.

[35] T. Wang, Y. Shen, A. Conti, and M. Z. Win, "Network navigation with scheduling: Error evolution," *IEEE Trans. Inf. Theory*, vol. 63, no. 11, pp. 7509–7534, Nov. 2017.

[36] X. Li, T. Zhang, W. Yi, L. Kong, and X. Yang, "Radar selection based on the measurement information and the measurement compensation for target tracking in radar network," *IEEE Sensors J.*, vol. 19, no. 18, pp. 7923–7935, Sep. 2019.

[37] N. Cao, S. Choi, E. Masazade, and P. K. Varshney, "Sensor selection for target tracking in wireless sensor networks with uncertainty," *IEEE Trans. Signal Process.*, vol. 64, no. 20, pp. 5191–5204, Oct. 2016.

[38] Z. Gao, C. Cecati, and S. X. Ding, "A survey of fault diagnosis and fault-tolerant techniques—Part I: Fault diagnosis with model-based and signal-based approaches," *IEEE Trans. Ind. Electron.*, vol. 62, no. 6, pp. 3757–3767, Jun. 2015.

[39] D. Simon, *Optimal State Estimation: Kalman, H Infinity, and Nonlinear Approaches*. Hoboken, NJ, USA: Wiley, 2006.

[40] J. Duník, O. Straka, O. Kost, and J. Havlík, "Noise covariance matrices in state-space models: A survey and comparison of estimation methods—Part I," *Int. J. Adapt. Control Signal Process.*, vol. 31, no. 11, pp. 1505–1543, Nov. 2017.

[41] G. Agamennoni, J. I. Nieto, and E. M. Nebot, "Approximate inference in state-space models with heavy-tailed noise," *IEEE Trans. Signal Process.*, vol. 60, no. 10, pp. 5024–5037, Oct. 2012.

[42] S. Wang, C. Li, and A. Lim, "A model for non-stationary time series and its applications in filtering and anomaly detection," *IEEE Trans. Instrum. Meas.*, vol. 70, pp. 1–11, Feb. 2021, Art. no. 6502911, doi: 10.1109/TIM.2021.3059321.

[43] R. Chartrand, "Numerical differentiation of noisy, nonsmooth data," *ISRN Appl. Math.*, vol. 2011, pp. 1–12, Jan. 2011.

[44] S. Aghabozorgi, A. S. Shirkhorshidi, and T. Y. Wah, "Time-series clustering—A decade review," *Inf. Syst.*, vol. 53, pp. 16–38, Oct. 2015.

[45] Z. Sahinoglu and S. Gezici, "Ranging in the IEEE 802.15. 4a standard," in *Proc. IEEE Annu. Wireless Microw. Technol. Conf.*, Dec. 2006, pp. 1–5.

[46] Y. Huang, Y. Zhang, N. Li, Z. Wu, and J. A. Chambers, "A novel robust student's t-based Kalman filter," *IEEE Trans. Aerosp. Electron. Syst.*, vol. 53, no. 3, pp. 1545–1554, Jun. 2017.

[47] W. Youn, Y. Huang, and H. Myung, "Robust localization using IMM filter based on skew Gaussian-gamma mixture distribution in mixed LOS/NLOS condition," *IEEE Trans. Instrum. Meas.*, vol. 69, no. 7, pp. 5166–5182, Jul. 2020.

Shixiong Wang (Graduate Student Member, IEEE) received the B.Eng. degree in detection, guidance, and control technology and the M.Eng. degree in systems and control engineering from the School of Electronics and Information, Northwestern Polytechnical University, Xi'an, China, in 2016 and 2018, respectively. He is currently pursuing the Ph.D. degree with the Department of Industrial Systems Engineering and Management, National University of Singapore, Singapore.

His research interests include statistics and optimization theories with applications in signal processing (especially optimal estimation theory) and control technology.

Zhongming Wu received the Ph.D. degree in management science and engineering from the School of Economics and Management, Southeast University, Nanjing, China, in 2019.

He is currently an Associate Professor with the School of Management Science and Engineering, Nanjing University of Information Science and Technology, Nanjing. His research interests include optimization theories and applications.

Andrew Lim received the B.Sc. and Ph.D. degrees in computer and information sciences from the University of Minnesota, Minneapolis, MN, USA, in 1987 and 1992, respectively.

He held professorships with the National University of Singapore, Singapore, The Hong Kong University of Science and Technology, Hong Kong, and the City University of Hong Kong, Hong Kong. He is currently a Project PI with the School of Computing and Artificial Intelligence, Southwest Jiaotong University, Chengdu, China, and the Chief Scientist with Red Jasper Holdings, Singapore. His research interests include big data analytics, digital twin, digital transformation, demand generation, and supply management problems in the domains of healthcare, logistics, and transportation.